GANIL

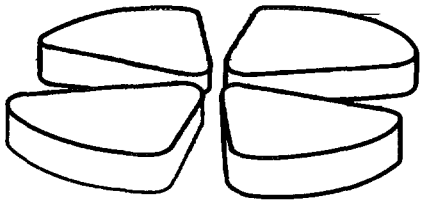

A simulation of the temperature distribution in the SPIRAL target.

R. Lichtenthäler[a,b], P. Foury[c], J. C. Angelique[d], P. Bertrand[a], B. Blank[e], O. Bajeat[c], M. Ducourtieux[c], P. Jardin[a], N. Lecesne[a], A. Lépine-Szily[b], M. Lewitowicz[a], C.F. Liang[f], M. Loiselet[g], H. Lefort[c], R. Leroy[a], J. Mandin[a], C. Marry[a], L. Maunoury[a], J. Obert[c], N. Orr[d], J.Y. Pacquet[a], J. C. Putaux[c], G. Ryckewaert[g], E. Robert[a], M. G. Saint-Laurent[a], P. Sortais[a], M. Toulemonde[h], I. Tirrel[a], A.C.C. Villari[a]

GANIL P 97 30

A simulation of the temperature distribution in the SPIRAL target.

R. Lichtenthäler[a,b], P. Foury[c], J. C. Angelique[d], P. Bertrand[a], B. Blank[e], O. Bajeat[c], M. Ducourtieux[c], P. Jardin[a], N. Lecesne[a], A. Lépine-Szily[b], M. Lewitowicz[a], C.F. Liang[f], M. Loiselet[g], H. Lefort[c], R. Leroy[a], J. Mandin[a], C. Marry[a], L. Maunoury[a], J. Obert[c], N. Orr[d], J.Y. Pacquet[a], J. C. Putaux[c], G. Ryckewaert[g], E. Robert[a], M. G. Saint-Laurent[a], P. Sortais[a], M. Toulemonde[h], I. Tirrel[a], A.C.C. Villari[a]

[a]GANIL, B.P. 5027, 14076 Caen Cedex 5, France

[b]Instituto de Física da Universidade de São Paulo, C.P. 66318, 05315-970, São Paulo, S.P., Brazil

[c]IPN Orsay, BP 1, 91406 Orsay, France

[d]LPC-ISMRa, Bld. Marechal Juin, 14050,Caen,France

[e]CENBG, B.P.120, 33175 Gradignan Cedex, France

[f]CSNSM, Bat104-108, 91406 Orsay, France

[g]CRC-IPN, Université Catholique de Louvain, B-1348 Louvain-La-Neuve, Belgium

[h]CIRIL, R.Claude Bloch, B.P. 5133, 14040 Caen cedex, France

August 1, 1997

Abstract

We developed a model and a computer program to calculate the temperature distribution in the target which will be used in the SPIRAL project at GANIL. The results of the numerical simulation are compared with measurements performed with several types of targets.

1 Introduction

The radioactive beams of the SPIRAL [1] project at GANIL will be produced by the nuclear reactions of the primary beam on a thick carbon target located outside an ECR ion source (SIRA-Radioactive Ions Separator). In order to have a fast diffusion of the unstable particles through the target material, it is necessary to heat the carbon target up to temperatures around $2400K$. Although these temperatures can be easily reached by heating due to a primary beam of 6kW, it is well known that the energy loss of heavy-ions is concentrated in a small region (Bragg peak) which makes the temperature profile in the target very non-uniform. Several experiments performed at GANIL have shown that under a heavy ion beam the target reaches temperatures near the sublimation point of the carbon. Due to the fact that the evaporation rate of carbon becomes too high at temperatures of the order of $2700K$, it is important to optimize the temperature profile as a function of the geometric parameters of the target. The solution adopted in order to obtain a more uniform temperature distribution was a target with a conic shape. The target developed consists of thin slices of carbon with an increasing radius, and separated by a certain distance. In this way, the energy loss near to the Bragg peak is distributed over several slices avoiding a localised overheating. The slices are connected to one and other through a central axis of carbon. If necessary, auxiliary ohmic heating is afforded either by an electric current through the central axis, or through an external container.

The difficulty of measuring the temperatures of the target near to the hot zone was the motivation for developing a model and a numerical simulation which should permit to calculate the temperature distribution in the target as a function of time due to the heating. We describe the model and compare the results of the numerical simulation with the measurements performed at Louvain La Neuve using a 6kW proton beam in a conic target, at ORSAY with ohmic heating, and at GANIL using a cylindric target hit by 400W ^{20}Ne and 200W ^{78}Kr beams.

2 The model and the numerical simulation.

In order to obtain the dynamic temperature distribution in the target, it is necessary to consider the heat diffusion equation with a source term which

accounts for the energy deposited by the incident beam. Due to the fact that the thermal conductivity and the specific heat of graphite depend strongly on temperature, and that the radiation boundary conditions have a temperature dependece as T^4, the problem becomes non-linear and can only be solved numerically [2]. The calculation is performed by the numerical integration of the non-linear differential equation in cylindrical coordinates:

$$\rho C(T)\frac{\partial T}{\partial t} = \frac{\partial}{\partial r}[k(T)\frac{\partial T}{\partial r}] + \frac{k(T)}{r}\frac{\partial T}{\partial r} + q_a + q_{rad} \qquad (1)$$

Where $T = T(z, r, t)$ is a function of the spatial coordinates and of the time t. ρ is the density of the target material, C its specific heat and k is the thermal conductivity all taken as a function of the temperature.

The first two terms in the right side of equation 1 account for the heat conduction in the radial direction. q_a is the energy density deposited per unity of time either by the beam, or by ohmic heating or both. More details about the heating will be presented in the next sections. q_{rad} describes the heat exchanges by radiation between neighbour slices. In fact equation 1 must be modified when the integration is performed over the central axis of carbon. In this case a term must be included $\frac{\partial}{\partial z}(k\frac{\partial T}{\partial z})$ which describes the conduction in the axial direction(z). Obviously there is no radiation between slices $(q_{rad}) = 0$ in this case. The element of volume considered in the integration is given by $dV = 2\pi rhe$ where h and e are the integration steps in the radial and axial directions respectively.

The slice is supposed to be thin and the integration step in the axial direction e is always taken equal to its thickness. This means that at a given radial position the temperature is the same at both faces of the slice and constant in the element of volume considered.

The time step of the integration is related to the integration step h and with the physical properties of the target material by the formula [2]:

$$\Delta t \leq \rho C h^2/(2k). \qquad (2)$$

This inequality imposes a time step of integration smaller than the time of propagation of the heat in the lattice. After a number of simulations with different target materials and integration steps we found that equation 2 gives a quite precise estimation of the time step necessary for convergence. For the carbon target this is of the order of milliseconds.

In order to label an element of volume in the target we define the index m and i such that $z = me$ and $r = ih$. At high temperatures the dominant mode of heating exchange is by radiation. The radiation term q_{rad} describes the heat exchange between one element of volume (i) of a given slice summed over all elements (j) of the neighbour slices:

$$q^{\pm}_{rad} = \frac{\sigma}{e} \sum_{j=1}^{jmax} \varepsilon_{ap}(i,j)(T^4_{m,i} - T^4_{m\pm1,j}). \tag{3}$$

The apparent emissivity between two rings ε_{ap} is calculated in appendix 1. No dependence with the temperature of the emissivities is assumed.

In order to solve the differential equation we follow the finite-difference method [3]. We set:

$$\frac{\partial T}{\partial r} = \frac{1}{2h}(T_{i+1} - T_{i-1}) \tag{4}$$

$$\frac{\partial^2 T}{\partial r^2} = \frac{1}{h^2}[(T_{i+1} - T_i) - (T_i - T_{i-1})] \tag{5}$$

and

$$\frac{\partial k}{\partial r} = \frac{1}{2h}(k_{i+1} - k_{i-1}). \tag{6}$$

The axial term is taken as:

$$\frac{\partial T}{\partial z} = \frac{1}{2e}(T_{m+1} - T_{m-1}) \tag{7}$$

and

$$\frac{\partial^2 T}{\partial z^2} = \frac{1}{e^2}[(T_{m+1} - T_m) - (T_m - T_{m-1})]. \tag{8}$$

2.1 Boundary conditions

Basically three situations must be examined concerning the boundary conditions for equation 1:

- For $i = 0$ (the center of the axis) we impose the temperature distribution to have an extremum:

$$\frac{\partial T_{m,0}}{\partial r} = 0 \tag{9}$$

we can write:

$$T_{m,1} = T_{m,0} + h\frac{\partial T_{m,1}}{\partial r} \tag{10}$$

which due to condition (9) yields:

$$\frac{1}{h}\frac{\partial T_{m,0}}{\partial r} = \frac{\partial^2 T_{m,0}}{\partial r^2} \tag{11}$$

and with the symmetry relation $T_{m,-1} = T_{m,1}$ we obtain:

$$\frac{\partial}{\partial r}[k\frac{\partial T_{m,0}}{\partial r}] + \frac{k}{r}\frac{\partial T_{m,0}}{\partial r} = \frac{4k}{h^2}(T_{m,1} - T_{m,0}) \tag{12}$$

- The target is surrounded by a cylindric container of carbon. We supose that the last ring of each slice radiates with the slice of the container immediately in front as a black body. We assume that all the heat emmited by the last ring is absorbed by the container at the position corresponding to slice m. For $i = i_{max}$ the heat density exchanged with the container is calculated by:

$$q = \frac{\varepsilon\sigma}{h}(T^4_{m,i_{max}} - T^4_{m,cont}). \tag{13}$$

- Each ring of each slice radiates either with the neighbour slices (equation 3) or with an exterior enclosure at a fixed temperature T_{sub}:

$$q = \frac{\sigma}{e}\varepsilon(T^4_{m,i} - T^4_{sub}). \tag{14}$$

2.2 The container and reflectors

Equation 1 is solved in order to calculate the temperature distribution in the container with the supposition that it absorbes all the heat emitted by the last ring of each slice m. In this way, the container has a differential distribution of temperature in the axial direction $T_{m,cont}$. In the radial direction the temperature of the container is assumed to be constant. The internal radius and thickness of the container are taken into account by renormalizing the heat density with the ratio of the volume elements: $q_c * dV_c = -q_l * dV$ where q_c and q_l are the heat densities absorbed by the container and emitted by the

last slice respectively. $dV_c = 2\pi r_c h_c e$ is an element of volume in the container of thickness h_c and radius r_c and dV is the element of volume in the last ring.

Each slice of the container radiates as a black body either with the enclosure at T_{sub} or with a reflector placed between it and the enclosure. In our calculation there is the possibility of considering up to 3 reflectors between the container and the substract. In all cases the temperature of the reflectors is assumed to be constant and given by [4]:

- 1 reflector

$$t_{el} = \frac{1}{m_{max}} \sum_{1}^{m_{max}} \left(\frac{\varepsilon_{cs} T_{cont}^4(m) + \varepsilon_{ss} T_{sub}^4}{\varepsilon_{cs} + \varepsilon_{ss}}\right)^{\frac{1}{4}} \tag{15}$$

  where ε_{cs} and ε_{ss} are the apparent emissivities between the container-reflector and the reflector-substract given by:

$$\varepsilon_{cs} = \frac{1}{\frac{1}{\varepsilon_c} + \frac{1}{\varepsilon_s} - 1} \tag{16}$$

- 2 and 3 reflectors

  The temperature of the first reflector is calculated for $n = 1, 2$ reflectors in the approximation $\varepsilon_s \ll \varepsilon_{c,s}$: [4]

$$t_{el} = \frac{1}{m_{max}} \sum_{1}^{m_{max}} \left(\frac{n T_{cont}^4(m) + T_{sub}^4}{n - 1}\right)^{\frac{1}{4}} \tag{17}$$

2.3 The heating process

The heating of the target can be made by both the beam and an electrical current.

- The Beam.

  The energy loss of each particle of the beam on each slice of thickness e is calculated by the program using routine ZSTOP[5]. The energy deposited by unit time and unit volume is given by:

$$q_a = N \frac{dE}{dx} \frac{f(r)}{\pi R_b^2} \tag{18}$$

where N is the total number of incident particles per unity time, $\frac{dE}{dx}$ is the electronic stopping power calculated by ZSTOP, R_b is the radius of the beam section, and $f(r)$ is a spacial distribution function which can be either square $f(r) = 1$ or gaussien:

$$f(r) = exp(-r^2/R_b^2) \tag{19}$$

Note that:

$$\frac{1}{\pi R_b^2} \int_0^\infty exp(-r^2/R_b^2) 2\pi r dr = 1 \tag{20}$$

- Rotating Beam

  A common way to control the target overheating is to use a rotating beam. In the case of a gaussien rotating beam, the argument of the exponential r^2 in equation 20 can be replaced by the effective distance between the center of the beam (which is now a function of time) and a certain element of volume m, i of the target:

$$r^2 \longrightarrow r^2 + r_0^2 + 2rr_0 cos(wt + \pi) \tag{21}$$

  where r_0 is the position where the center of the beam hits the target and w is the angular frequency of rotation. If the frequency of rotation is not very high compared to the integration time step, this procedure gives a good approximation for the heat density effectively received by a certain element of volume of the target as a function of time during one rotation. For the typical case of $\Delta t = 0.001s$ frequencies up to $100Hz$ are acceptable. For higher frequencies of rotation this procedure can introduce numerical errors.

- Ohmic heating

  In the case where the energy density deposited by the beam is not sufficient to heat the target up to operating temperatures a system of heating by electric current is desirable. If an electrical current density

J passes through the axis, the heat density in each element of volume is given by:

$$q_a = \rho_{el} J^2 \tag{22}$$

where ρ_{el} is the electrical resistivity of the target material and $J = \frac{I}{\pi r_{axis}^2}$.

- Total incident power

  For monitoring purposes the program integrates the total incident power during one interation time step separetely for the beam and the ohmic heating. This is given by:

$$P = \sum_{m=1}^{mmax} \sum_{i=1}^{imax} q_a(i,m) dV \tag{23}$$

  For the case of a rotating beam, the power density q_a is a function of the time and an average over one period $T = 2\pi/w$ is performed.

3 Applications of the numerical simulation.

3.1 The Conic Target and a 6kw proton beam.

Figure 1 presents the conic target used for the tests perfomed at Louvain-La-Neuve with a 6kW proton beam. The target is made of one single piece of carbon of 9.4cm length by 4.3cm diameter. It consists of 33 slices (20 slices in the conic part and 13 slices in the cylindric part) of thickness 0.07cm separated by 0.13cm. The total angle of the cone is of 45 deg. The slices are connected to each other by an axis of 5.8mm external diameter and 3mm internal diameter which allows the insertion of a thermocouple in order to measure the temperature along the axis. 1cm of axis is without slices. An electrical current through the axis provides the auxilary heating. In the rear there is a solid part which has the double function of fixing the target in the internal walls of a cylindrical container and making the electric contact for the return of the electric current, which is made by the container. The entire system target and container is placed inside a chamber kept at a constant temperature ($T_{sub} \approx 290K$) by a water refrigerating system.

The cyclotron of Louvain-La-Neuve provided the proton beam of 30MeV and power from 0 to 6kW. The beam rotates with a frequency of 50Hz. The radius of rotation of the beam can be varied and was of about 1.25cm during the experiment. The beam current was integrated in the target throughout the whole experiment providing a measurement of the incident power. Due to the difficulty of monitoring a 6kW proton beam, the beam profile was not measured. The beam size was adjusted at the begining of the experiment by inserting a slit of 1.5cm diameter in front of a low power beam and adjusting the focalization in order to achieve 70% of transmission through the slit. The slit is then removed and the beam power increased. For the simulations we made the assumption that the beam was gaussien with a FHWM of 1.7cm. This parameter is very important in order to determine the temperature of the target in the region of the Bragg peak. The smaller the width of the beam, the higher the temperature will rise near to the Bragg peak. Hence a precise measurement of the beam width is necessary if we wish to control the maximum target temperature.

The target temperature was measured by 3 thermocouples placed respectively in the axis, in the slice at $r = 1.7$cm from the axis and in the container. The three thermocouples were at the same axial position ($z = 6.2$cm), which means approximately slice 27.

As a first test we performed measurements of the time of response of the target which consisted of exposing the target, initially cold, to the beam power and measuring the temperature in intervals of 3 seconds until reaching the temperature of equilibrium T_{max}. After that, the beam was cut off and we observed the cooling back to the room temperature. This was done for 3 beam powers 0.8kW, 1.7kW and 3.8kW and the results are presented in figures 2, 3 and 4 (dashed line) with the simulation (solid line). We observed that the rise time is shorter for the higher beam powers. If we define the rise time as the time needed to reach 90% of the maximum temperature we obtain $t_{rise} = 205s, 300s, 456s$ respectively for $3.8kW, 1.7kW, 0.8kW$. On the other hand, the decaying time up to room temperatures is much longer, of the order of $600s$. This behaviour can be understood in terms of the interplay between the conduction and the radiation regimes. For lower temperatures the radiation term q_{rad} in equation 1 is small and the dynamic is determined mainly by the conduction. As the temperature increases the conductivity of the carbon decreases and the conduction becomes negligible compared to the radiation term. In this situation the heat propagation through the target be-

comes faster. It is important to take this fact into account in the simulation, mainly at low incident powers which would require a longer calculation time to converge.

The conductivity of the carbon used in the simulation was measured by the [6] in the range 273K to 1800K where it apparently reaches a minimum. Above this temperature we assumed a constant thermal conductivity equals to the minimum value. The emissivity of the carbon was assumed constant, equal to the unity.

The accord between measurements and simulation are quite good. The rise and decaying times are very well reproduced. The calculated equilibrium temperature in the slice is a little above the measured. It is necessary to mention that the measurements on the axis are overestimated due to the fact that a fraction of the beam hit this thermocouple. In reality the temperature of the axis is almost the same as the temperature measured in the slice, in agreement with the results of the simulation. This fact can be observed comparing the measurements in the region with no beam ($t \geq 850$s). The discrepancies observed at low temperatures of the container are due to the threshold of this thermocouple ($600K$).

In figure 5 we present the temperature profile obtained by the simulation with a 6kW beam. We observe that the Bragg peak is spread over a region parallel to the cone. The highest temperature in this situation is approximately $2600K$ and very high temperature gradients are observed. In the region around $z \approx 6$cm (slice 27), the temperature gradient in the axial direction is about $50\,\mathrm{deg}/mm$. On the other hand, the gradients in the radial direction are very low, as predicted by the simulation and confirmed by the measurements.

The examination of the target after the experiment has shown the presence of holes from the slice 10 up to 20, not in the direction of the beam but parallel to the cone of the target. It proves that the holes were caused by overheating along the Bragg peak. Temperatures of about $2700K$ in the Bragg peak are sufficient to evaporate a thin slice of 0.7mm in a few hours [8]. A more uniform profile is needed to operate in a long term with $6kW$ heavy ions beam. It can be obtained by decreasing the angle of the cone, for instance an angle of 30 deg gives a maximum temperature of $2500K$ in the Bragg peak.

3.2 The Conic Target and the ohmic heating.

In principle, the energy deposited in the target by a heavy ion beam of a few kilowatts is sufficient to heat the target up to temperatures of 2400K in the region around the Bragg peak. However, the range of nuclei produced by projectile fragmentation can be considerably longer than that of the beam, if we are interested in nuclei distant from the projectile. The necessity of additional ohmic heating comes mainly from the fact that we observed large temperature gradients in the axial direction. The ohmic heating can be done either by the central axis or by the container. The heating by the container has the advantage of providing a more uniform temperature profile but very high powers are required to heat a target of the dimensions of the SPIRAL. For this reason we adopted the axial heating.

We performed measurements at IPN-ORSAY with a conic target of 8.4cm long 2.2cm of diameter and a total angle of the cone of 20 deg. The heating was made by an electric current through the axis of power variable up to a maximum of 2300W. There was a tantalum reflector between the target and the container. The target temperature was measured by a pyrometer and thermocouples. The pyrometer measured the temperature in the front surface of the target in the radial direction and the thermocouples along the axis and in the container. The measurements of the temperature in the radial direction show a quite uniform profile with temperatures of about 1800K at the maximum power in very good accord with the simulation. However in the axial direction the measurements showed a temperature gradient much higher than the simulation which had predicted an almost uniform profile with decreasing temperatures only very near to the ends of the target. The reason for this discrepancy is probably due to the container which had a large radiating surface in its rear part, which was not considered in the simulation. If we consider a container 1cm thick, the results approach very much the measurements as shown in Fig. 6. Other possibilities, as points of contact with the cold chamber and the heat exchanges with the thermocouple, do not seem to be the main reason for the observed gradient. We believe that a container with a smaller radiating surface and thickness should give a more uniform axial temperature distribution. In particular, measurements performed in a cylindrical target heated by the container showed that the temperatures are quite uniform in the axial direction.

3.3 The cylindric Target.

Experiments have been performed at GANIL using beams of ^{20}Ne and ^{78}Kr of powers $400W$ and $200W$ [7] respectively and a cylindric carbon target of 2cm diameter and 4.2cm length also made of slices of 0.07cm thick separated by 0.1cm. The FWHM of the beams was 0.74cm, measured during the experiment. The target was heated by the container up to a temperature of $2300K$. These temperatures were attained due to reflectors placed between the container and the refrigerated chamber. After the experiment a conic shape hole was observed in the target hit by the ^{20}Ne beam (Fig. 7). The hole started at slice 8 up to slice 20 and had a maximum diameter of $\approx 6mm$ at slice 13, which is the position of the Bragg peak for the 95MeV.A ^{20}Ne. There was no hole in the target hit by the ^{78}Kr beam. The shape of the hole is basically due to the gaussien shape of the beam and its process of formation can be undertood if we address to equation 18. There are two effects to be considered: one due to the stopping power dE/dz which increases with z reaching a maximum at the Bragg peak and the other due to the beam intensity which decreases with r^2 for a gaussien beam. If we assume that there is a certain value of power density q_a^L, above which a hole will be formed, it is easy to understand that the hole should start at some place before the Bragg peak where the smaller energy loss is compensated by the high energy densities at small radius. As we approach the Bragg peak the energy loss increases and the limit value q_a^L will be reached respectively for increasing radii up to the Bragg peak where the radius is maximum. Obviously, as a hole is formed, the beam will heat the next slice and the hole propagates beyond slice 13. A stationary situation is attained when the energy is distributed over several slices forming a cone. The angle of the cone follows the Bragg peak and can be considered as an estimation of the optimum angle for a conic target. In this case the angle is of about 30 deg.

We performed a simulation which included the possibility of the formation of a hole. This was done by setting a limit temperature above which a hole is supposed to be formed. During the simulation, the temperature of a given position is kept fixed as it reaches the limit, and the corresponding energy loss of the beam will be deplaced to the next slice. The result of the simulation for a limit temperature of $2700K$ is shown in Fig. 8. The black region corresponds to the region where the temperature exceeds the limit of $2700K$ and a hole is supposed to be formed. The shape and dimensions of the hole

obtained by the simulation are very similar to those observed experimentally. The maximum temperature attained by the target in the simulation is of $2800K$, which is below the sublimation point of graphite (3300K). It indicates that the hole is not formed immediately but that a certain time is necessary to evaporate the carbon. Of course the time to form a hole depends on the beam characteristics, as its width which strongly influences the maximum temperatures in the target. The closer these temperatures are from the sublimation point of the carbon, the faster the evaporation process will be.

The simulation performed for the target in the case of the ^{78}Kr beam resulted in a maximum temperature of $2500K$, well below the $2800K$ for the ^{20}Ne case in accord with the experiment.

4 Conclusions

We developed a model and a computer code to calculate the temperature distribution in the SPIRAL target. The calculation simulates the process of heat propagation in the target as a function of time due to a rotating beam or an electric current. The simulation was applied to the cases of conic and cylindric targets made of thin slices of carbon. The comparison with the experimental measurements performed at Louvain-La-Neuve with a 6kW proton beam, at GANIL with ^{20}Ne and ^{78}Kr beam, and at IPN-ORSAY with ohmic heating, show that the simulation reproduces quite well the observed features. In particular the dynamics of the temperature evolution in the target as a function of time is well reproduced. The calculated absolute temperatures are a little above the measurements performed with thermocouples at some points of the target however the temperatures around the Bragg peak seem to be very well predicted. More precise calculations would require precise measurements of the physical properties of the target material as the thermal conductivity and emissivities in the region of high temperatures.

If we suppose that above $2700K$ the evaporation rate of the carbon becomes very high ([8]), the position and the dimensions of the damage observed in the targets used at Louvain-La-Neuve and at GANIL are very well reproduced by the simulation.

A large temperature gradient has been observed in the conic targets with ohmic heating by the central axis. This diagnostic obtained by the simulation indicates that the container should be the main reason for this gradient

in particular the large radiating area of the container in its rear part. A new design for the container with a smaller radiating area and thickness is desirable.

In summary the calculation seems to be very useful for predicting the limits of resistance of targets to the heating caused by nuclear beams as well as by other forms of heating. It is also very useful for determining the influence of variations of the geometric parameters of the target in the temperature profile, allowing an optimization of these parameters.

5 Appendix

The heat exchanged by radiation between to elements of surface dS_i and dS_j and emissivities ε_i and ε_j is given by:

$$q_{ij} = \frac{\sigma(T_j^4 - T_i^4)}{\frac{1-\varepsilon_i}{\varepsilon_i dS_i} + \frac{1-\varepsilon_j}{\varepsilon_j dS_j} + \frac{1}{f_{ij} dS_i}}. \tag{24}$$

where f_{ij} is the form factor between dS_i and dS_j and the term which multiplies $\sigma(T_j^4 - T_i^4)$ we call apparent emissivity.

The form factor is calculated by:

$$f_{ij} = \frac{1}{\pi S_i} \int\int \frac{dS_i \cos\Theta_{ij} dS_j \cos\Theta_{ji}}{d_{ij}^2} \tag{25}$$

where Θ_{ij} is the angle between the normal to the surface i and the line d_{ij} which connects the two surfaces.

Calculation of the form factor between two coaxial rings

The form factor of two disks of radius R_1 and R_2, separated by a distance h_x is given by:[9]

$$f_{12} = \frac{1}{2}(x - \sqrt{x^2 - 4(\frac{R_2}{R_1})^2}) \tag{26}$$

where

$$x = 1 + \frac{(h_x^2 + R_2^2)}{R_1^2} \tag{27}$$

We can show that the form factor between two rings of thickness $\Delta R1 = R_j - R_i$ and $\Delta R_2 = R_l - R_k$ can be calculated from F_{ij} via the relation:

$$F_{12} = \frac{S_j(f_{jl} - f_{jk}) - S_i(f_{il} - fik)}{S_1} \tag{28}$$

where:

$$S_j = \pi R_j^2 \tag{29}$$

$$S_i = \pi R_i^2 \tag{30}$$

$$S_1 = \pi R_1^2 \tag{31}$$

References

[1] The SPIRAL Radioactive Beam Facility, GANIL Report **R-94-02**, Caen (1994); A.C.C. Villari and the SPIRAL group, Nucl. Phys. **A616**, 21c (1997)

[2] M. Toulemonde, C. Dufour, E. Paumier
Physical Review **B46** $n°22$ 14362 (1992)

[3] H.S. Carslaw and J.C Jaeger, Conduction od Heat in Solids (Oxford University, New York,1959)

[4] Techniques de l'Ingénieur, Genie Industriel(thermique)
A1 820-18

[5] STOPX code by W.T. Milner
ORNL-USA using the formulas and parameters of J.F. Ziegler,
The Stopping and Ranges of Ions in Matter - Pergamon Press (1980)

[6] Groupe CARBONE LORRAINE -Specialties and Advanced Materials
BP 148 -41, rue Jean Jaurès
F. 92231 Gennevillers -France

[7] N. Lecesne - PHD thesis - GANIL - 1997(in progress)

[8] J.C. Puteaux, P. Bertrand, M. Ducourtieux, A. Ferro, P. Foury, O. Kaitasov, L. Kotfila, N. Lecesne, R. Leroy, C.F. Liang, M. Loiselet, J. Mandin, L. Maunoury, A.C .Mueller, J. Obert, J.Y. Paquet, N. Pauwels, J.C. Potier, J. Proust, E. Robert, M.O. Ruault, G. Ryckewaert, P. Sortais, M. Toulemonde, A.C.C. Villari.
Nucl. Instr. and Methods in Phys. Res. **B126**, 113(1997)

[9] Techniques de l'Ingénieur, Genie Industriel(thermique)
A3, **A1 520**-21

Figure 1: Conic carbon target used at Louvain-la-Neuve.

Figure 2: Temperature as a function of time measured(dashed) and calculated(solid) in the slice(up), axis(middle) and container(down) for 0.8kW beam power.

Figure 3: Temperature as a function of time measured(dashed) and calculated(solid) in the slice(up), axis(middle) and container(down) for 1.7kW beam power.

Figure 4: Temperature as a function of time measured(dashed) and calculated(solid) in the slice(up), axis(middle) and container(down) for 3.8kW beam power.

Figure 5: Temperature profile obtained by the simulation for a 6kW proton beam.

Figure 6: Temperature in the axis(up) and container(down) of the conic target as a function of the axial position with ohmic heating.

Figure 7: Cylindric target used at GANIL with 95MeV.A ^{20}Ne beam. The cone represents the hole found in the target after radiation.

Figure 8: Result of the simulation for the cylindric target. Region in black represents the hole predicted by the simulation.

Target Louvain-97

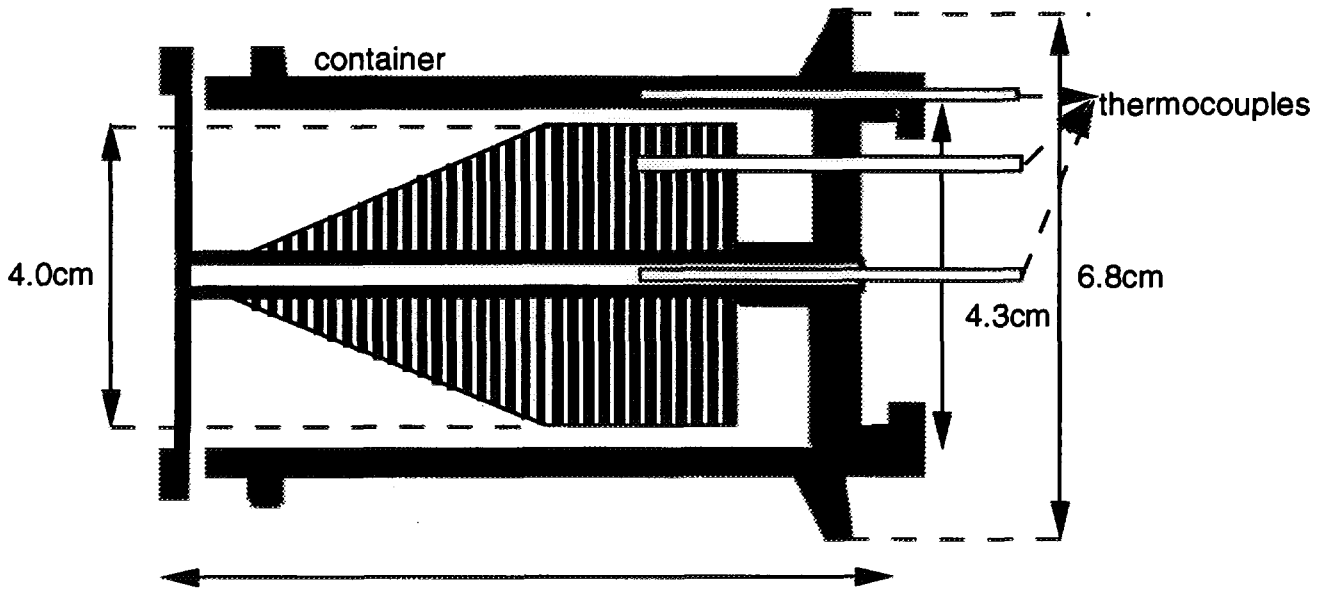

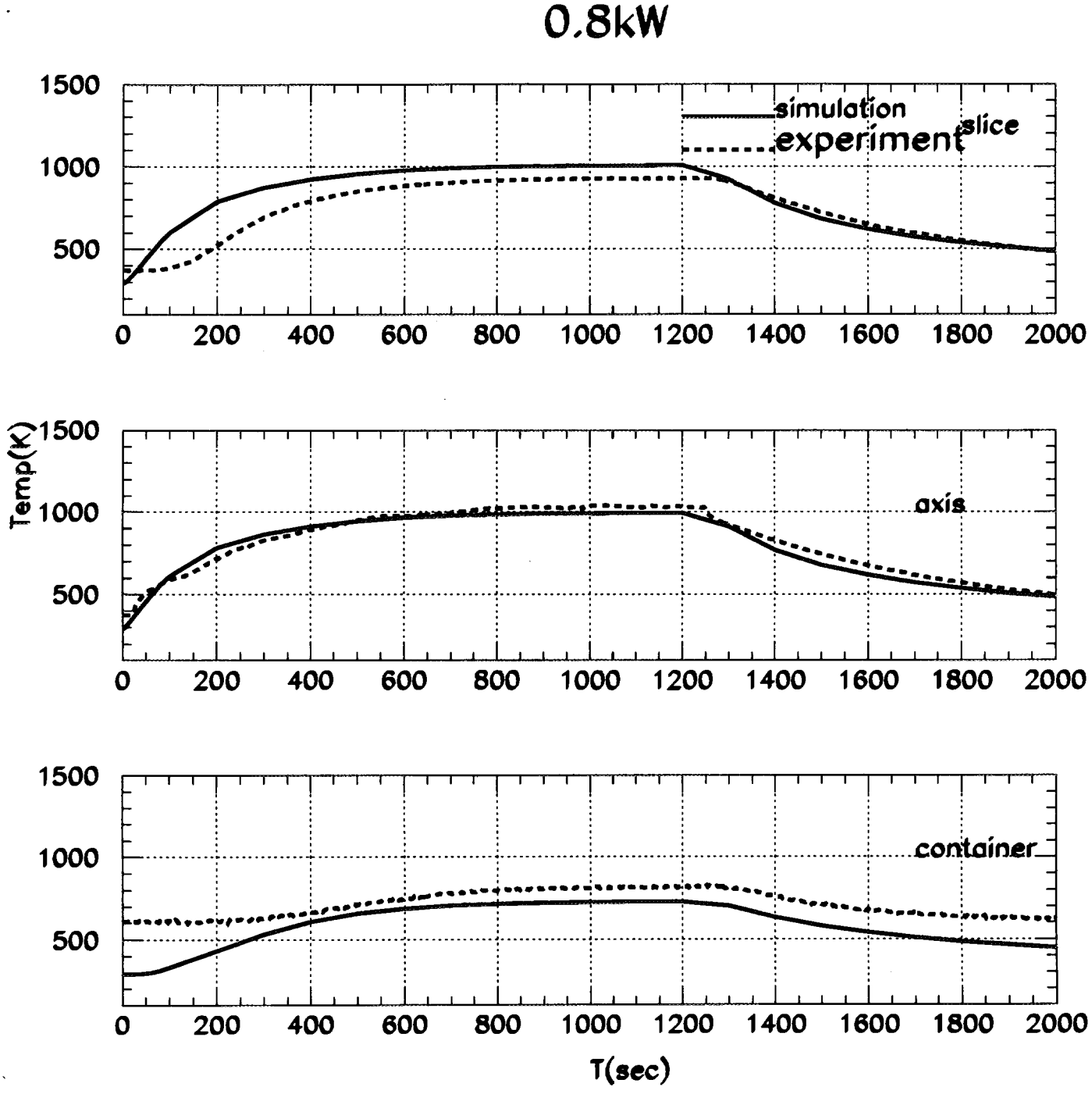
0.8kW
simulation
experiment
slice
axis
container
Temp(K)
T(sec)
1500
1000
500
0
200
400
600
800
1000
1200
1400
1600
1800
2000

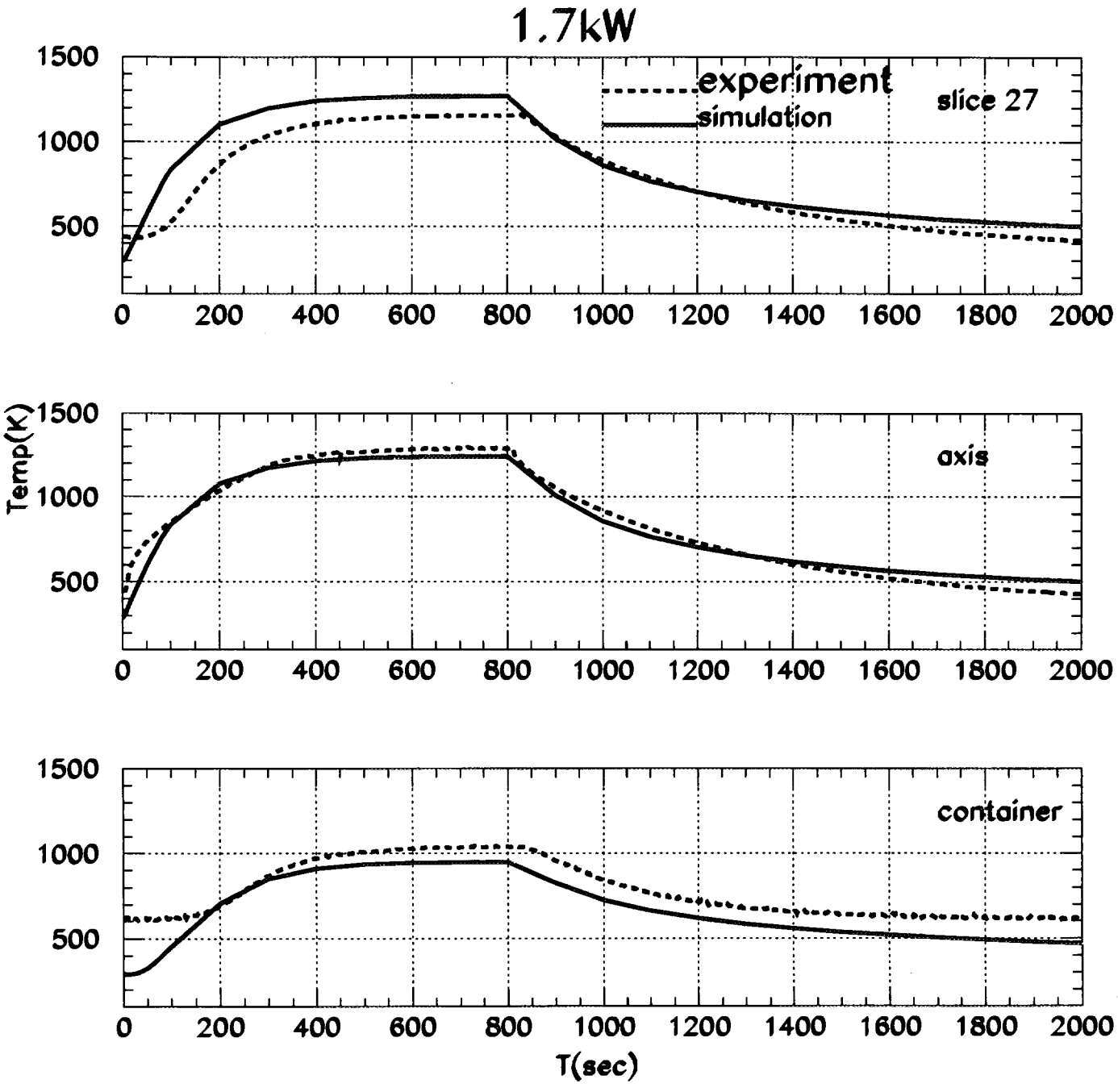
1.7kW
experiment
simulation
slice 27
axis
container
Temp(K)
T(sec)
1500
1000
500
0
200
400
600
800
1000
1200
1400
1600
1800
2000

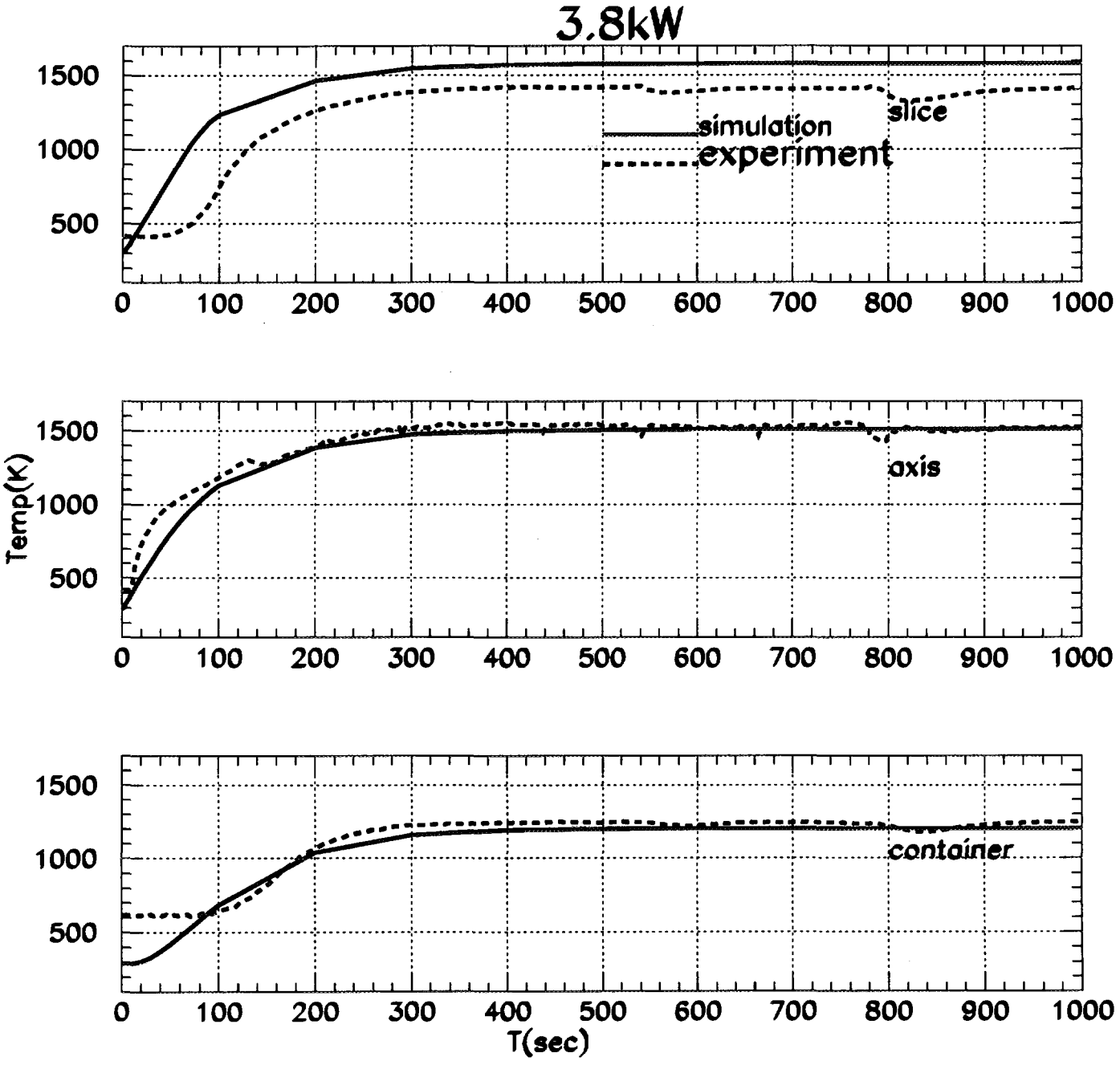
3.8kW
1500
1000
500
0
100
200
300
400
500
600
700
800
900
1000
simulation
experiment
slice
axis
container
Temp(K)
T(sec)

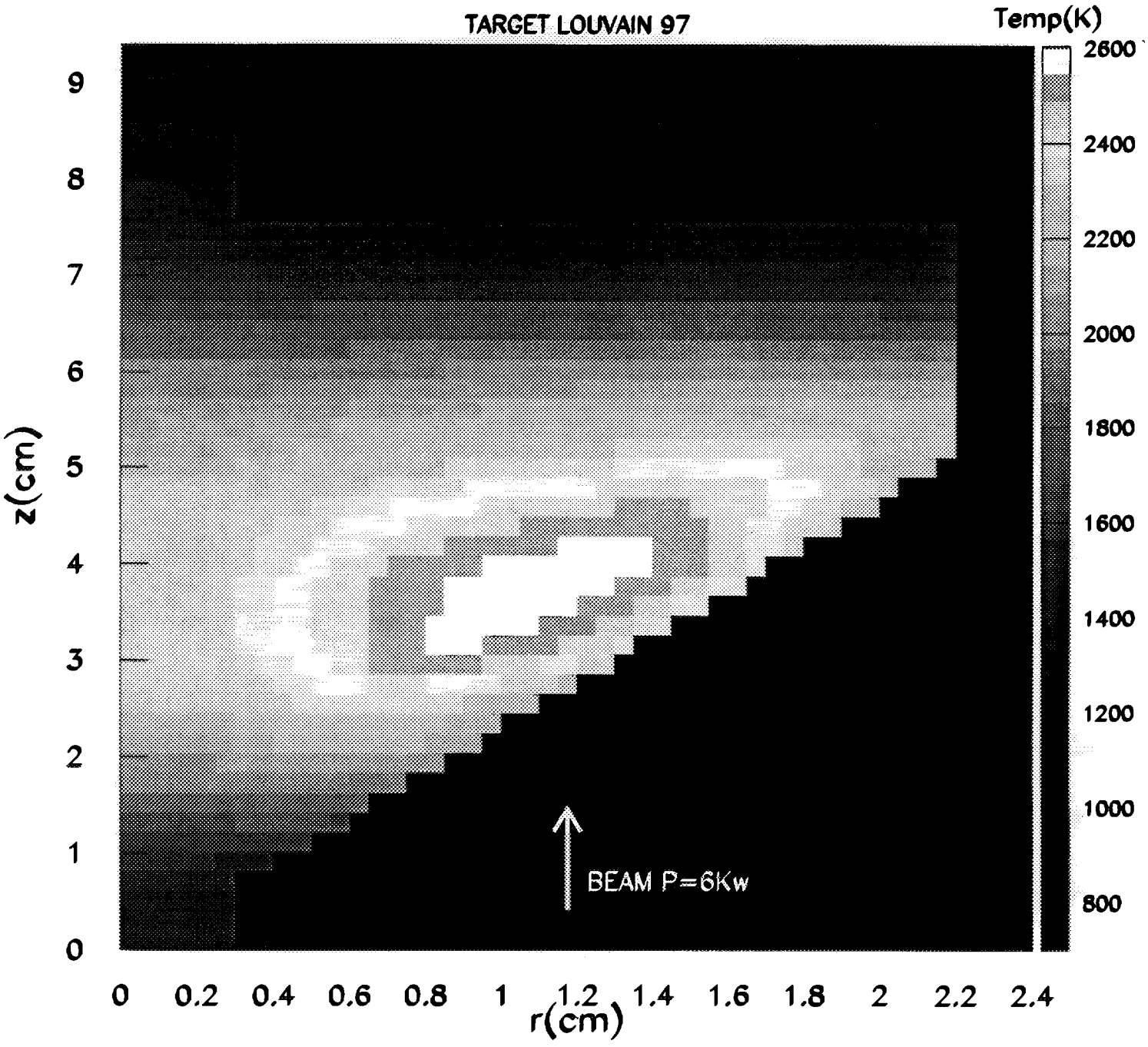
TARGET LOUVAIN 97
Temp(K)
2600
2400
2200
2000
1800
1600
1400
1200
1000
800
z(cm)
0
1
2
3
4
5
6
7
8
9
BEAM P=6Kw
0
0.2
0.4
0.6
0.8
1
1.2
1.4
1.6
1.8
2
2.2
2.4
r(cm)

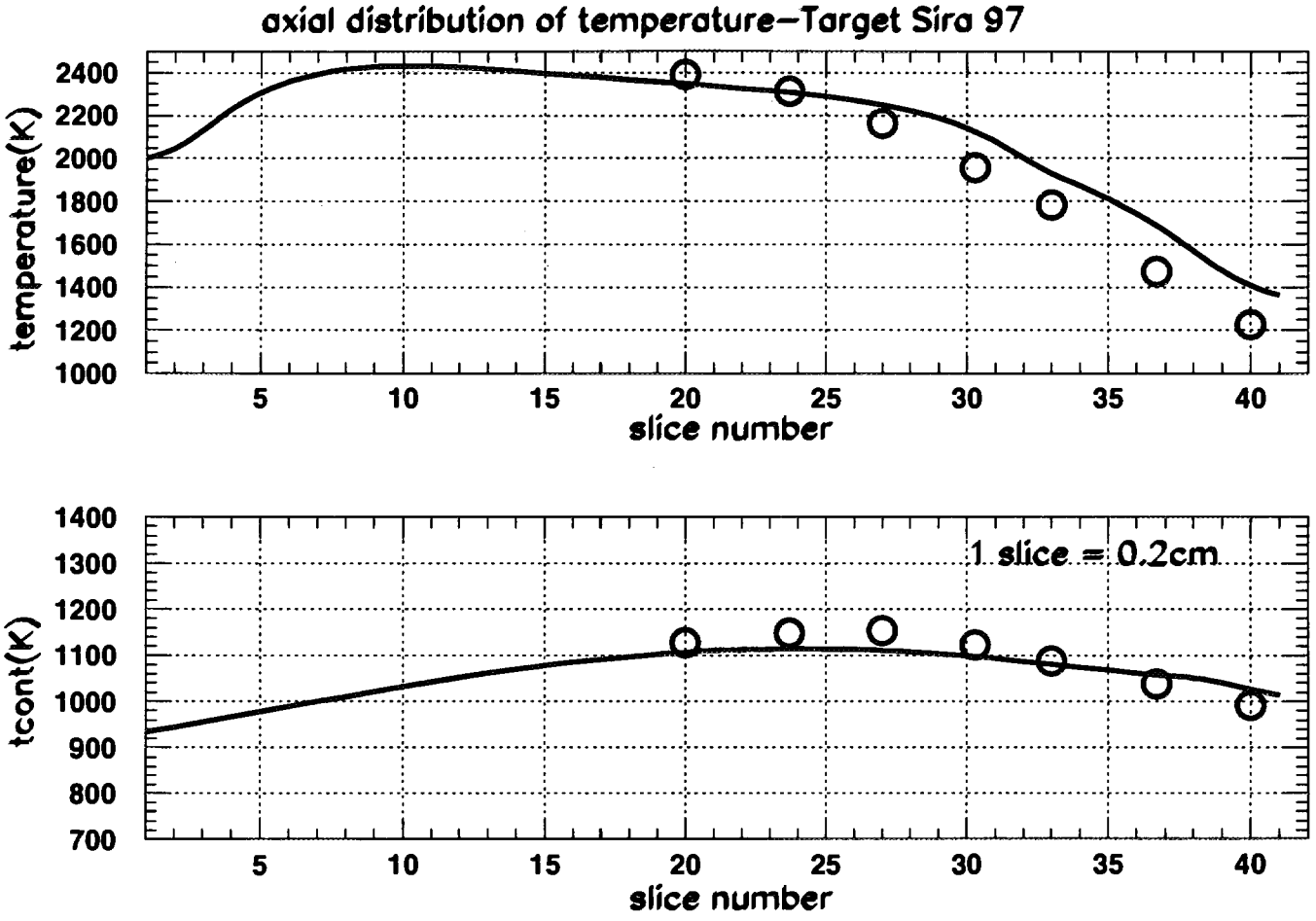
axial distribution of temperature–Target Sira 97
temperature(K)
2400
2200
2000
1800
1600
1400
1200
1000
5
10
15
20
25
30
35
40
slice number

tcont(K)
1400
1300
1200
1100
1000
900
800
700
1 slice = 0.2cm
5
10
15
20
25
30
35
40
slice number

cilindric target

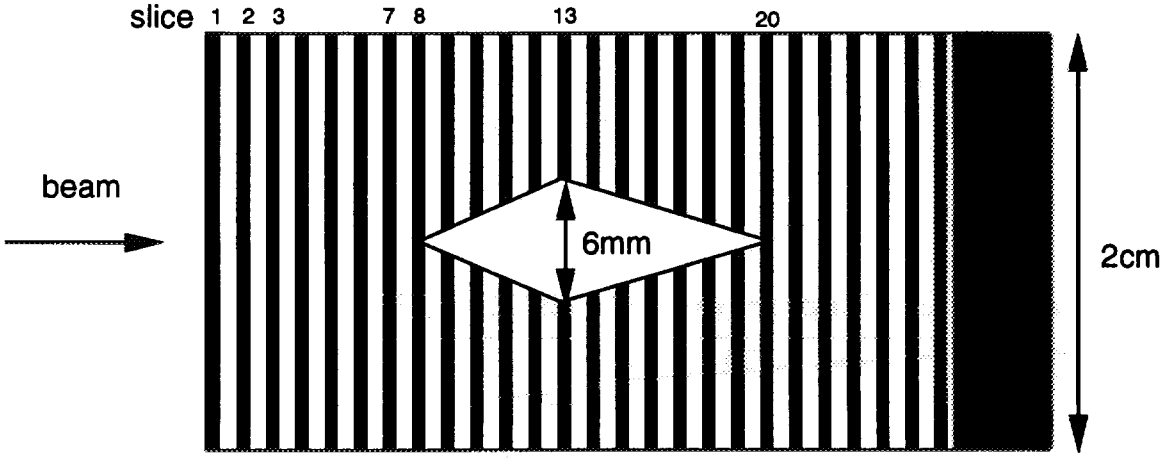

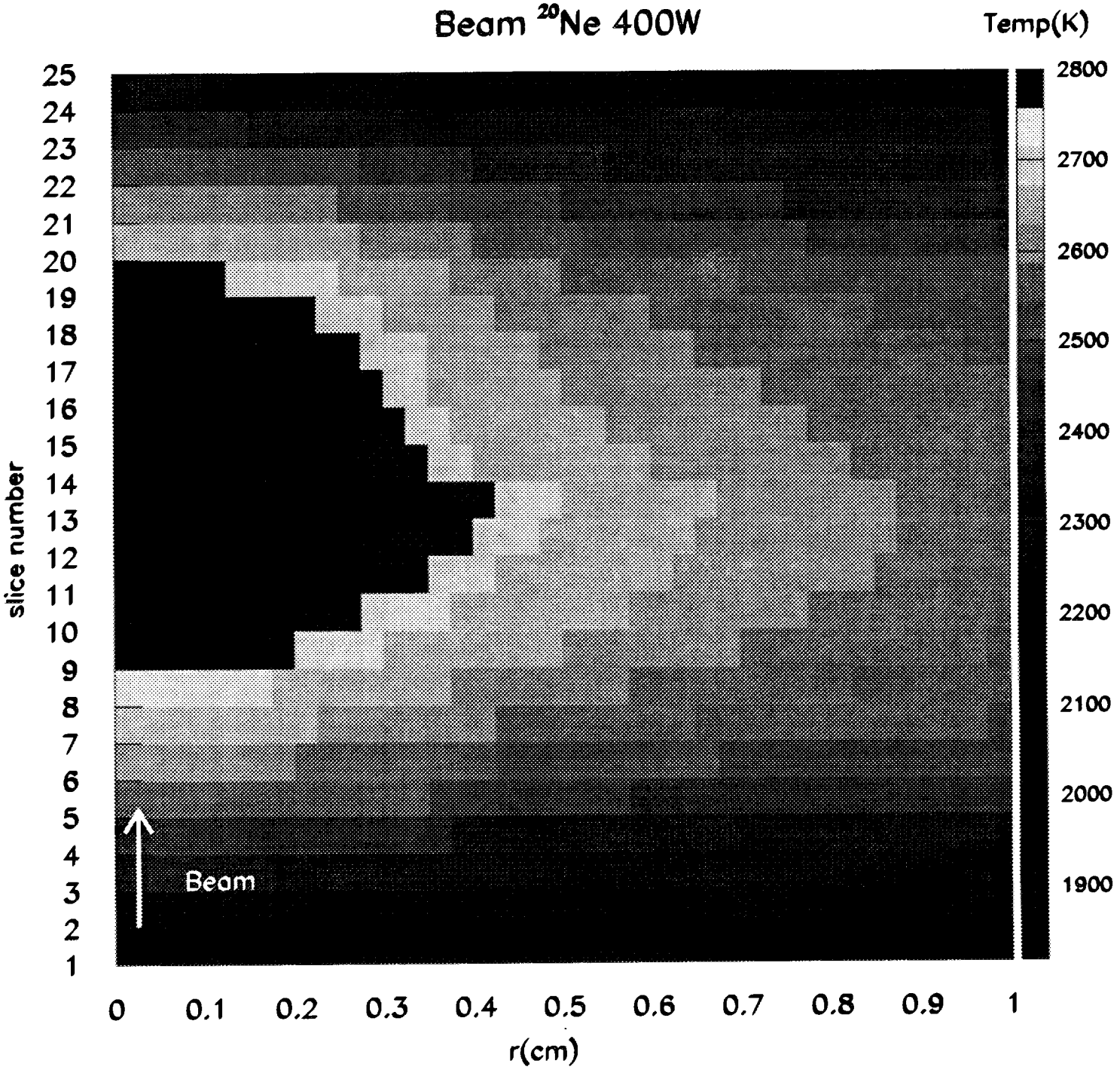
Beam ^{20}Ne 400W
Temp(K)
2800
2700
2600
2500
2400
2300
2200
2100
2000
1900
slice number
25
24
23
22
21
20
19
18
17
16
15
14
13
12
11
10
9
8
7
6
5
4
3
2
1
Beam
0
0.1
0.2
0.3
0.4
0.5
0.6
0.7
0.8
0.9
1
r(cm)